Pergamon International Journal of Machine Tools & Manufacture 41 (2001) 1209–1228

INTERNATIONAL JOURNAL OF MACHINE TOOLS & MANUFACTURE DESIGN, RESEARCH AND APPLICATION

The application of high-speed CNC machining to prototype production

Tony Schmitz [a,*], Matthew Davies [a], Brian Dutterer [a], John Ziegert [b]

[a] *Manufacturing Metrology Division, National Institute of Standards and Technology, MS 8220, Gaithersburg, MD 20899, USA*

[b] *Machine Tool Research Center, Department of Mechanical Engineering, University of Florida, Gainesville, FL 32611, USA*

Received 10 March 2000; accepted 5 December 2000

Abstract

This paper describes the application of high-speed milling to the production of monolithic, metallic, functional prototypes, with special emphasis placed on the applicable process times. An example component is selected and the relevant process times are presented. Fundamental requirements for the use of high-speed milling to produce prototypes in a timely manner are identified. These requirements include: 1) high speed/high power spindles, 2) proper spindle speed selection based on the system dynamics, 3) machining parameter definition based on tool wear, 4) high feed/high acceleration machine drives, 5) intelligent path generation, and 6) pre-process verification of arbitrary three-dimensional CNC part paths. The implementation of the Simultaneous Trilateration Laser Ball Bar (STLBB) system to measure the CNC part paths is described and the device verification procedure is outlined. Example two and three-dimensional path measurements are also shown.

Keywords: High-speed machining; Dynamic measurements; Prototypes

1. Introduction

Methods for the timely manufacture of prototypes for design verification and/or modification have recently focussed on a number of rapid prototyping techniques (e.g., stereolithography apparatus, solid ground curing, selective laser sintering, laminated object manufacturing, and fused deposition modeling, among others). These techniques are typically additive processes that pro-

* Corresponding author.
E-mail address: tony.schmitz@nist.gov (T. Schmitz).

0890-6955/01/$ - see front matter
PII: S0890-6955(01)00005-0

duce engineering prototypes in minimum possible lead times [1–8]. In stereolithography apparatus, for example, a three-dimensional (3-D) computer-aided design (CAD) model is divided into several thin cross-sections, these individual layers are deposited using a photosensitive liquid polymer and directed laser beam one at a time until the solid part is complete, and the part is cured by exposure to ultraviolet light (light sanding is also sometimes required). The use of computer numerically-controlled (CNC) machining, a subtractive process, to produce prototypes has been generally disregarded due to the increased time and cost over other available processes. In the research described here, methods to improve the efficiency of CNC machining (i.e., shorten the manufacturing cycle time and reduce process expense) are detailed in an attempt to adapt this process to the production of functional, metallic (e.g., aluminum, carbon steel, nickel aluminum bronze, titanium alloys, nickel superalloys, hardened die steel) prototypes.

2. High-speed milling

As noted previously, machining is a subtractive process. In order to produce the final, 3-D product, material must be successively removed from a solid workpiece. Therefore, in order to decrease the machining cycle and resulting prototype lead times, the time to traverse the consecutive contours (machining passes) must be decreased and/or the amount of material removed during each pass must be increased. The method of high-speed milling (HSM) attempts to address both of these issues.

The implementation of HSM requires an understanding of the system dynamics, cutting force interactions at the tool-chip interface, and the rate of tool wear. The system dynamics impact the allowable stable material removal rate (MRR). Theory and experimental verification have shown that the limiting stable axial depth of cut (for a given radial immersion, feed, and workpiece material) is highly dependent on the selected spindle speed and frequency response of the tool/machine/workpiece system. A graphical explanation of this phenomenon has taken the form of stability lobe diagrams [9,10]. In Fig. 1, it is seen that the chatter-free axial depth of cut (b_{lim})

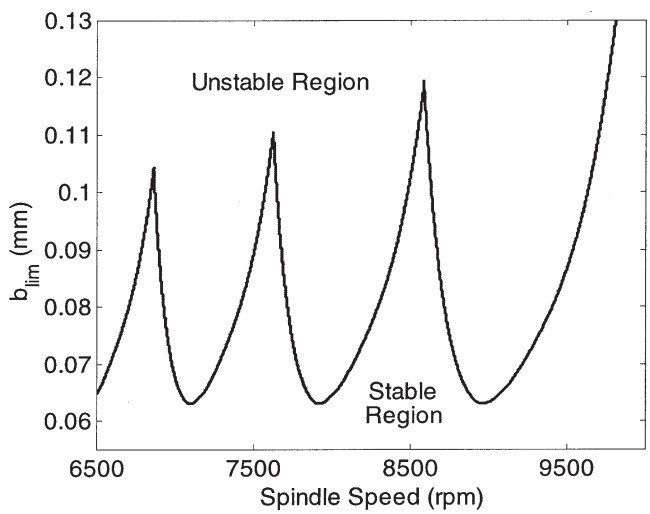

Fig. 1. Example stability lobe diagram.

varies substantially with spindle speed. Dramatic increases in b_{lim}, and therefore the material removal rate, are observed at specific speeds. These most favorable tooth passing frequencies (spindle speeds) for process stability occur when operating at a substantial integer fraction of the natural frequency that corresponds to the most flexible mode of vibration of the structure [11–13].

The ability to accurately model the tool-chip interface during intermittent machining (milling) is necessary for the formulation of analytical and/or numerical process simulations that do not rely heavily on empirical information. Currently, many models require an experimental determination of the *cutting force coefficients* that provide a fairly crude representation of the chip formation process and are specific to the workpiece material, tool geometry, and cutting conditions. These modeling efforts [14] are aimed at replacing the previous method of selecting machining parameters from large, difficult-to-maintain, empirical databases (e.g., [15]).

Tool wear is considered a function of the thermal, stress, and strain-rate conditions at the tool-chip interface. Chip formation under the high strain-rate, high-temperature conditions found in HSM may lead to a transition from continuous to shear-localized (oscillatory) material flow and limit the process efficiency in many hard-to-machine materials [16,17]. The effect of workpiece material on attainable cutting speeds (circa 1992) is demonstrated in Fig. 2 (after Schultz and Moriwaki [18]). Clearly, the definition of *high-speed* in the term high-speed machining is material dependent.

Another important consideration in HSM is the capabilities of the machining center. In order to take advantage of the favorable spindle speeds shown in Fig. 1, a machine tool must be designed which incorporates a spindle with both high speed and high power capabilities (the current commercial state of the art is approximately 40,000 rpm/40 kW) with high feed/high acceleration, low mass drives. The high performance drives are necessary to rapidly traverse the commanded contours and keep the chip load high, even with the multiple starts and stops found in pocketing routines, for example (see Fig. 3). This combination of high feedrate (in excess of 0.6 m/s) and high acceleration (20 m/s^2) axes with a high speed/power spindle (and proper spindle speed selection) can provide a dramatic decrease in machining time.

When coupled with appropriate CAD/CAM technology (intelligent tool path generation, e.g., [19–23]), the use of HSM enables many monolithic parts to be produced in aluminum, nickel aluminum bronze, titanium alloys, nickel superalloys, or even hardened die steel [16] in less time

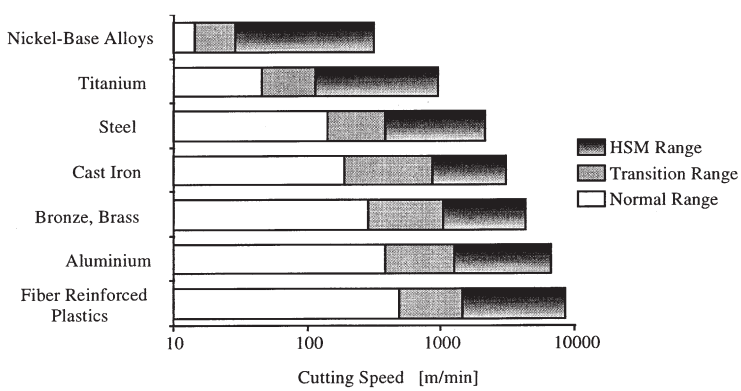

Fig. 2. Attainable surface speeds in the machining of various materials (After Schultz and Moriwaki [18]).

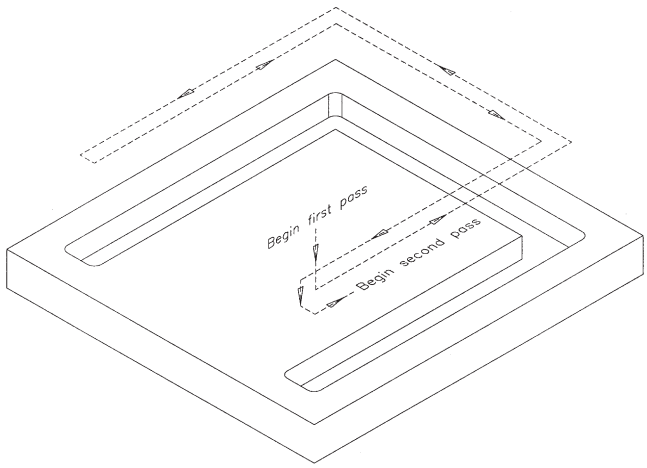

Fig. 3. Example pocketing routine.

than most rapid prototyping machines can make a layered composite plastic mock-up. In this sense, HSM may be considered *a single step process capable of producing functional (metallic) prototypes from three-dimensional computer models* [1,24–27].

At this time, the most dramatic applications of high-speed milling have been in the manufacture of aluminum components where volumetric material removal rates can approach thousands of cubic centimeters per minute. In the aerospace industry, for example, HSM is changing the way aircraft are manufactured by enabling the replacement of sheet-metal assemblies with machined monolithic components resulting in substantial cost savings and improved performance [28]. These monolithic structures can be stronger, lighter, and more accurate than the sheet-metal build-ups and provide a substantial reduction in inventoried jigs and fixtures.

The application of HSM to prototype production (and concurrent engineering) would also benefit from high-throughput machining (HTM) techniques [29]. HTM seeks to reduce the non-cutting portion of the manufacturing time by automatic part loading/unloading, in-process inspection and sensing, and adaptive control. A reduction in non-cutting time (and the corresponding increase in process efficiency) is especially important when high tool wear rates (associated with hard-to-machine materials) limit the efficiency of HSM.

2.1. Example: prototype production using high-speed milling

In order to demonstrate the prototyping capabilities of HSM, a generic test part has been defined and manufactured on a commercially available high-speed machining center (20,000 rpm/20 kW spindle). Production times (including programming, machine setup, and machining) and machining conditions were recorded. The results are tabulated in the following paragraphs.

The generic prototype geometry and nominal dimensions are given in Fig. 4. This part features a raised contour (10:1 height to thickness ratio) oriented on a small base (98.2 mm square by 25 mm thick). The selected material is 6061-T6 aluminum, although many other metallic/non-metallic materials may also be chosen.

A CAD drawing of the part was completed and the data file was delivered to the high-speed

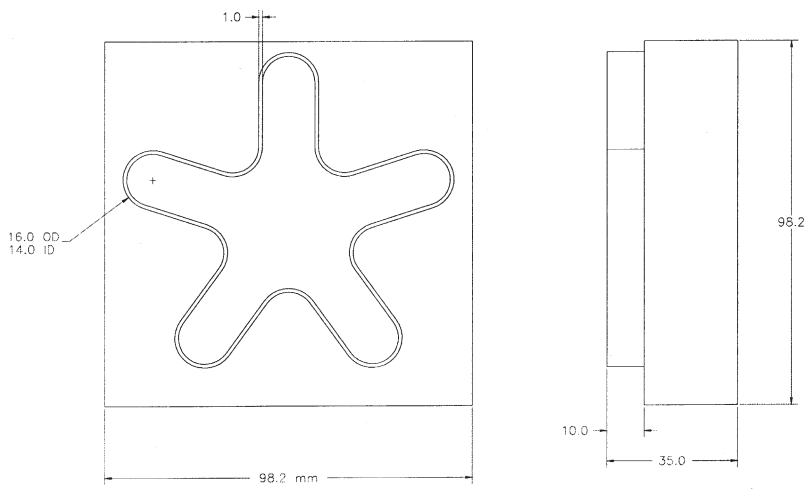

Fig. 4. Prototype geometry.

machinist. For this part geometry, the machinist selected a two flute, 12.7 mm diameter, 45.2 mm overhang tungsten carbide endmill (from the tooling already in place on the machine used in this study). The frequency response of this tool in the two orthogonal feed directions (x and y) was measured using impact testing (i.e., a modally tuned hammer was used to excite the tool point and the vibratory response recorded using a low mass, wide bandwidth accelerometer) and the modal parameters for the dominant modes were extracted (this procedure took approximately 45 min, but only needs to be completed once per tool). The results are shown in Table 1, where f_n is the natural frequency, k is the modal stiffness, and ζ is the modal damping ratio. The modal parameters were then used as input to a stability lobe analysis as described in the previous paragraphs. The stability lobe diagram for the measured tool is shown in Fig. 5 [10]. This plot shows that the optimum spindle speed for maximized MRR is 19291 rpm with a maximum stable axial depth of cut of approximately 10 mm for slot milling in aluminum.

The machinist next completed the NC programming for the prototype using a commercially available software package (approximately 10 min from supplied CAD drawing to NC path generation) and rather conservative machining conditions. Two part programs were completed and downloaded to the machining center. One program carried out the machining of the contoured

Table 1
Cutting tool modal parameters

	f_n (Hz)	k (N/m)	ζ
X direction	2578	4.2×10^7	0.023
	3076	8.5×10^6	0.016
	3290	4.0×10^7	0.025
Y direction	2560	4.3×10^7	0.025
	3070	9.0×10^6	0.020
	3288	2.9×10^7	0.023

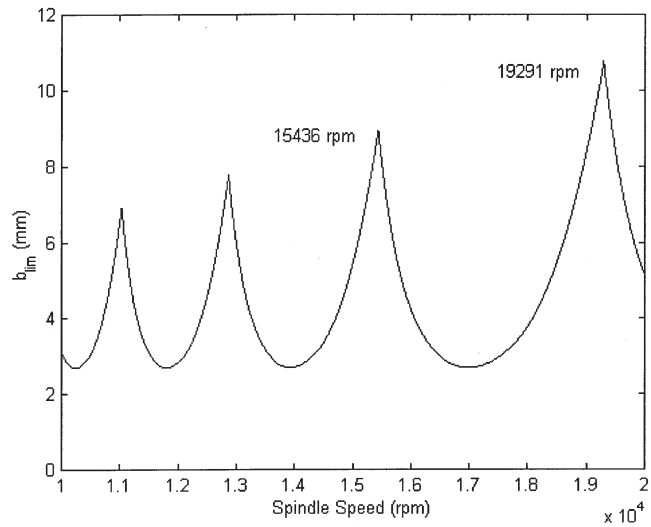

Fig. 5. 12.7 mm diameter, 45.2 mm overhang tool stability lobe diagram.

face and sides of the part and a second was responsible for facing the back of the part. The first program included a pocketing section for the raised contour (19291 rpm spindle speed, 4.6 m/min linear feed, and 5.0 mm axial depth of cut at full radial immersion) and a second section for reducing the outer periphery of the workpiece blank to the required dimensions (19291 rpm spindle speed, 4.6 m/min linear feed, and 7.6 mm axial depth at 40% radial immersion). The second program was composed of two facing passes at the same spindle speed and feed with 4.7 mm axial depth at full radial immersion of the tool.

A 108 mm square by 44.5 mm thick blank (roughly $3 material cost for 6061-T6 aluminum) was then loaded into the machine vise and an edge finder used to locate the blank within the machine's work volume (approximately 2 min). Next, the first part program was executed to machine the raised contour and sides of the part (<6 min). Finally, the part was flipped and the back faced using the second part program (2 min). The process times are summarized in Table 2. Although this is a contrived example with relatively simple geometry (the machined part is

Table 2
HSM process times

Process Description	Time (min)
NC programming	10
Part loading/locating	2
Program 1 execution	6
Program 2 execution	2
Total	20

shown in Fig. 6), it does provide a dramatic illustration of the possible savings in process time (and prototype lead time) when operating a high-speed machine tool under optimum conditions, even for modest material removal rates (a volume of 275,000 mm^3 was removed in under 8 min).

3. Pre-process CNC contour verification

If CNC machining is to be used for prototype production under time-sensitive conditions, it is important that the accuracy of the part program (i.e., the digitized prototype) can be verified without the necessity of machining a test part. In general, the manufacture of a new part by CNC machining includes: 1) defining the CNC part program using engineering drawings, 2) executing the part program in up to six coordinated axes to machine a test part or prototype, and 3) inspecting the test part, normally with the aid of a coordinate measuring machine, to check for conformance to design tolerances. This feedback of the actual part dimensions (with an adequate degree of precision) includes errors introduced by the environment, machine geometry, contouring accuracy, and the cutting process and is currently the only way to certify the overall performance of a given CNC program. If the test part does not meet the specified tolerances, as is often the case for a first trial, the CNC program is modified, another test part is machined, and the process repeated. This iterative post-process inspection is not acceptable if HSM is to be used in prototype manufacturing. In this situation, it is important to be able to verify the CNC part program prior to machining a costly and time-consuming test part.

At this time there are no commercially available sensors which are capable of the measurement of arbitrary, dynamic, 3-D contours to micrometer-level accuracy. Although laser trackers can perform 3-D dynamic measurements, these measurements have a standard uncertainty of roughly 10 μm, an order of magnitude larger. Therefore, a sensor has been developed which can measure these real-time CNC contours to the required level of accuracy[1] (over some finite portion of a

Fig. 6. Machined prototype.

[1] The design and testing of this instrument have been described previously [30]. However, as a convenience to the reader, we will include a brief description in the following paragraphs.

machine tool's work volume). When these contouring measurement results are coupled with other known systematic error sources (e.g., thermal, parametric, cutting force, tool wear, fixturing [31]), a pre-process description of the final part dimensions may be obtained.

3.1. Sensor description

The Simultaneous Trilateration Laser Ball Bar (STLBB) [32] system is based on the Laser Ball Bar (LBB), a precision linear displacement measuring device developed by Ziegert and Mize [33]. It consists of a two-stage telescoping tube with a precision sphere mounted at each end. See Fig. 7. A heterodyne displacement measuring interferometer is aligned inside the tube and measures the relative displacement between the two sphere centers.

The heterodyne signal (Helium–Neon, two frequency laser light) is carried from a frequency-stabilized laser head to the Michelson-type interferometer by a single-mode, polarization-maintaining (SMPM) fiber. At the LBB, a local reference is generated to eliminate cable-induced phase shifts (e.g., mechanical or thermal deformations) in the SMPM fiber. The local reference and measurement signals are carried to the phase-measuring electronics (after passing through a polarizing filter oriented at 45° to the two orthogonal frequencies to provide interference) via two multimode (MM) optical fibers. The final linear displacement is calculated by taking the difference of the measurement and local reference signals. The LBB has been shown to be accurate to submicrometer levels during static measurements [34]. Fig. 8 displays the optics package located in each LBB.

Because the linear displacement interferometer is only able to measure changes in displacement and not absolute distance, each LBB must be initialized to determine the sphere center-to-sphere center length prior to use. The (self) initialization procedure is composed of three steps. First, the LBB is placed between sockets 1 and 2 of the initialization fixture and the displacement counter zeroed. Next, the LBB is extended from socket 2 to 3 and the displacement recorded (after atmospheric correction). This displacement is the distance between sockets 2 and 3. Finally, the LBB is placed between sockets 2 and 3 and the length of the LBB initialized to the previously recorded displacement (see Fig. 9). The entire procedure takes approximately one minute, so any length changes in the initialization fixture due to thermal fluctuations are minimized.

Once initialized, the LBB uses trilateration to measure the spatial coordinates of points along a CNC part path. The six edges of a tetrahedron formed by three base sockets (rigidly attached

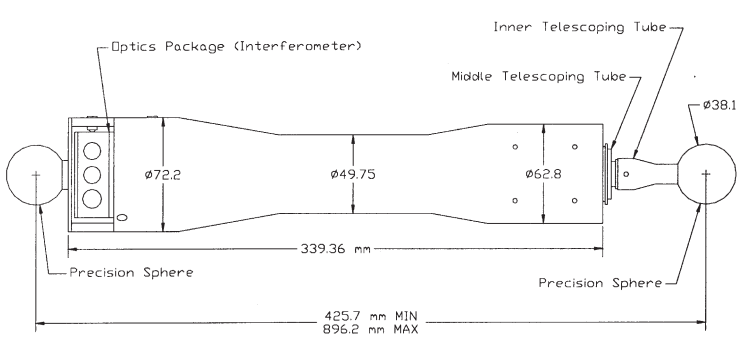

Fig. 7. Laser ball bar.

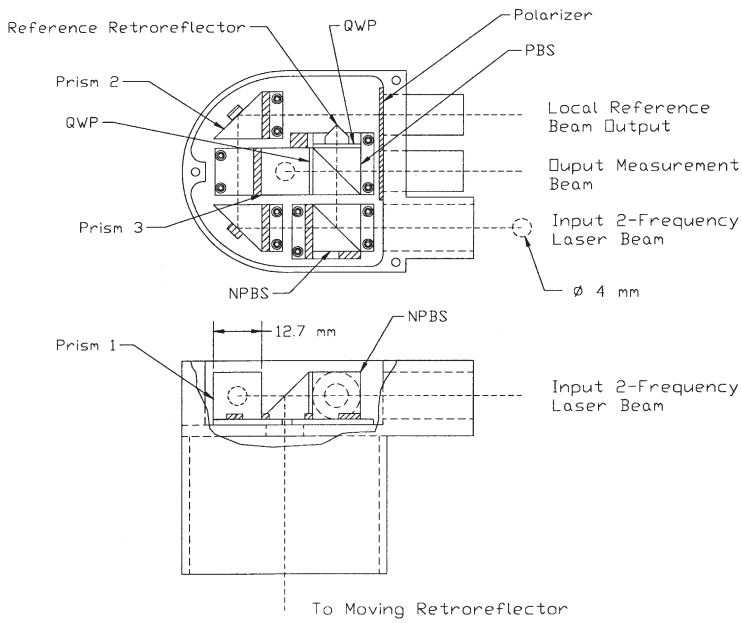

Fig. 8. LBB optics package.

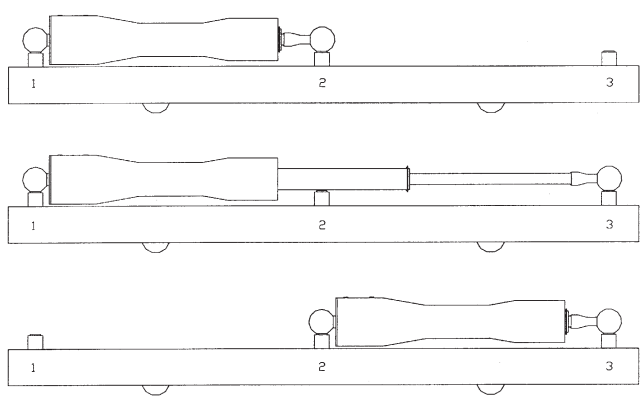

Fig. 9. LBB initialization procedure.

to the machine table) and a tool socket (mounted in the spindle) are measured and, by geometry, the spatial coordinates of the tool position in the LBB coordinate system are calculated. The three lengths between the three base sockets (L_{B1}, L_{B2}, L_{B3}) shown in Fig. 10 are measured once and are assumed to remain fixed during the motion of the tool socket.

The three base-to-tool socket lengths (denoted L_1, L_2, L_3 in Fig. 10) are measured simultaneously during a single execution of the applicable CNC part program. The experimental setup for simultaneous trilateration is shown in Fig. 11 (note that all three LBBs ride on a single precision sphere at the tool point). Simultaneous trilateration requires that the axes of the three LBBs meet at a single point that coincides with the tool point (to minimize Abbé offset errors).

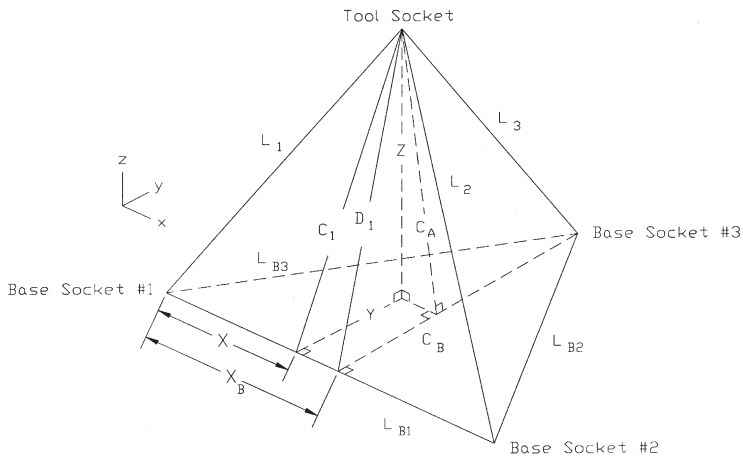

Fig. 10. Trilateration tetrahedron.

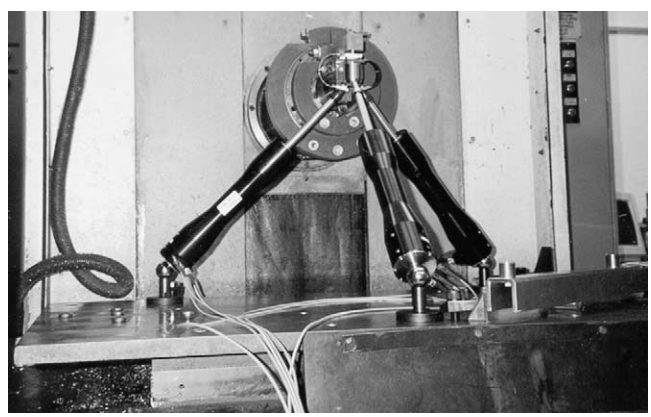

Fig. 11. Simultaneous trilateration.

During the execution of a CNC part program, the coordinates of the tool point are measured at closely spaced intervals along the path to define the contouring accuracy. As the spatial coordinates of the tool point vary, the lengths of the individual LBBs change as well as the angles between the LBBs. This calls for a joint which provides three independent angular degrees of freedom while prohibiting relative translations between the endpoints of each of the three LBB axes (e.g., a spherical joint).

3.2. Sensor verification

The first step in the verification of this sensor was to compare the STLBB results with those of an independent sensor under the same measurement conditions. Ideally, a verification device would be selected which could measure the same 3-D dynamic contours as the STLBB system. However, the best commercially available sensor was an optical grid encoder capable of 2-D

dynamic measurements. The grid encoder used in this research was provided by the Heidenhain Corporation.[2]

The Heidenhain KGM 101 Grid Encoder is composed of a grid plate (140 mm diameter) with a waffle-type grating of closely spaced lines (4 μm signal period) and a non-contact scanning head which is able to measure translations in two directions. The optical grid plate is attached to an aluminum mounting base. This base is mounted in the plane to be measured (on an *x*-*y* table for instance) and the scanning head is fixed perpendicular to the plate (e.g., on the *z* axis attached to the spindle). This system measures the relative planar motion of the two bodies for any curvilinear path in the plane of the mounting base with a resolution of 4 nm and manufacturer-specified standard uncertainty of 2 μm. The recorded motions allow the user to observe the dynamic effects of the machine tool's performance on 2-D CNC tool paths. Fig. 12 shows the setup used for the grid encoder 2-D measurements.

Several planar contours were selected for measurement with both the Heidenhain grid encoder and STLBB system. These contours and the pertinent dimensions are summarized in Fig. 13. During the experimental verification procedure, all paths were executed at constant accelerations (i.e., trapezoidal velocity profiles) of 0.98 m/s^2 to 4.91 m/s^2 with feedrates ranging from 889 mm/min to 1778 mm/min and spatial coordinate sampling was completed at a nominal rate of 1 kHz for both devices. Comparisons between two example Heidenhain and STLBB measurements will now be presented.

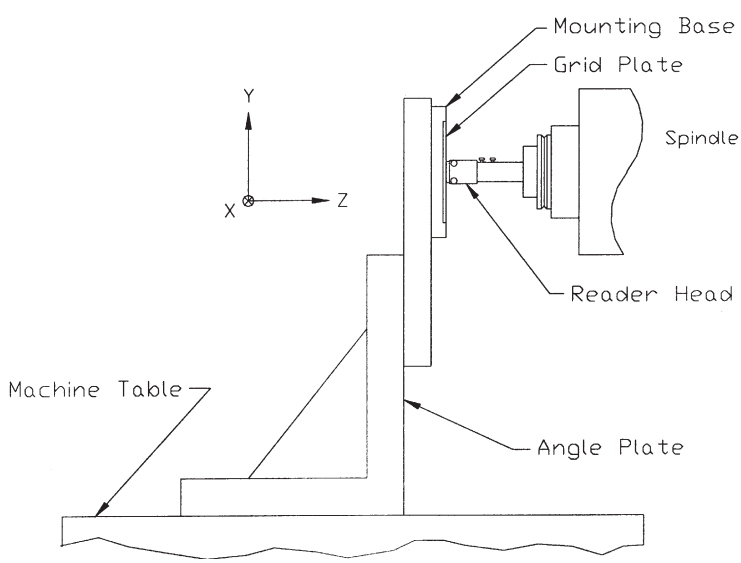

Fig. 12. Heidenhain grid plate setup.

[2] Commercial equipment is identified in order to adequately specify certain procedures. In no case does such identification imply recommendation or endorsement by the National Institute of Standards and Technology, nor does it imply that the equipment identified is necessarily the best available for the purpose.

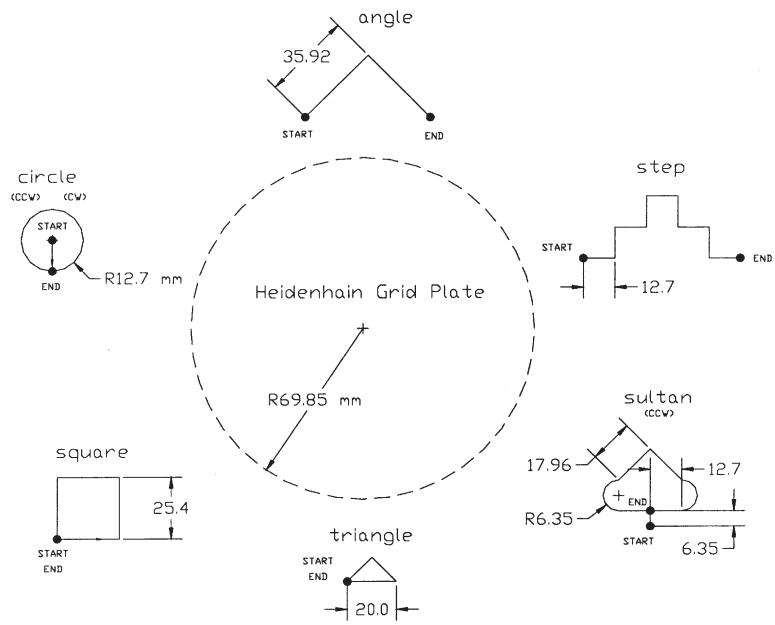

Fig. 13. STLBB verification contours.

3.2.1. Angle path

The angle path includes motions in the *x*-*y* plane which require linear interpolation in the two axes simultaneously. Fig. 14 shows a comparison between the Heidenhain grid plate and STLBB measurements for a feed of 889 mm/min and an acceleration of 0.98 m/s^2. Only the cornering portion of the much larger path is shown to enhance the viewing resolution. Fig. 15 exhibits the two measurements for a feed of 1778 mm/min and an acceleration of 4.91 m/s^2.

This path aids in the tuning of the servomotors on machine tools. The measured response (e.g., undershoot or overshoot) can be used to set the individual axis gains. For the machine tool used in this research, a difference in the gain between the *x* and *y* axes caused a steady-state positional error. Therefore, the actual contour is spatially offset from the commanded contour during constant velocity motion. Because this error is proportional to the commanded feedrate, the offset is seen to be larger in Fig. 15 than in Fig. 14.

3.2.2. Circle path

Clockwise and counter-clockwise circular paths were also measured using the two measurement systems. Fig. 16 displays the measurement results for a counter-clockwise circle with a commanded velocity of 1778 mm/min, where the radial deviations of the measured path from the commanded have been amplified by a factor of five. The figure shows an elliptical distortion of the path with the major axis of the ellipse rotated 45° counter-clockwise from the positive *y* axis. In this case, this elliptical distortion of the circular path was caused by the previously mentioned gain mismatch between the *x* and *y*-axes.

The good agreement between the optical grid plate and STLBB results for the angle and circle paths shown served to verify the overall dynamic performance of the STLBB system. However,

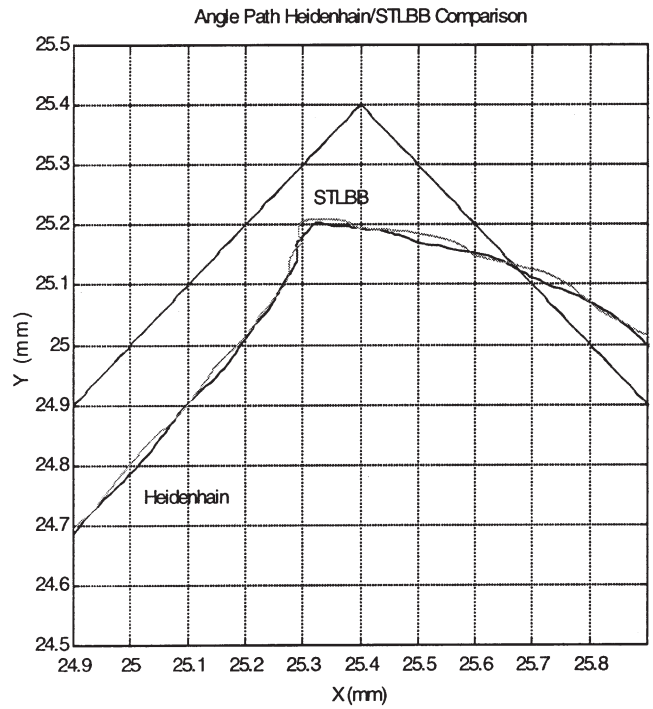

Fig. 14. Angle path comparison (889 mm/min, 0.98 m/s^2).

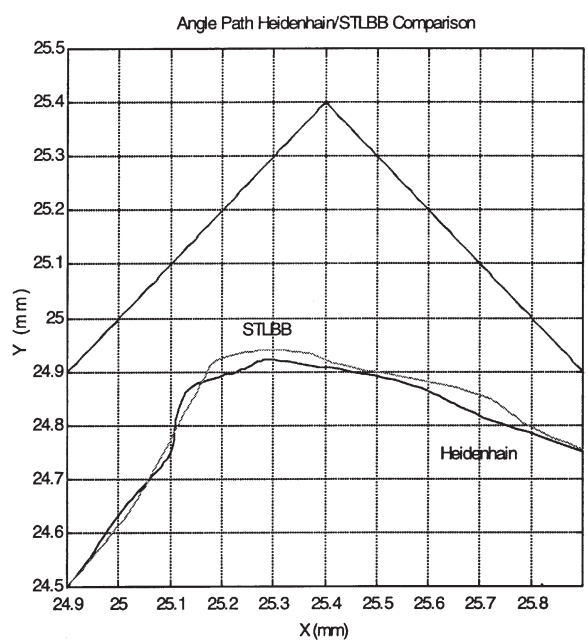

Fig. 15. Angle path comparison (1778 mm/min, 4.91 m/s^2).

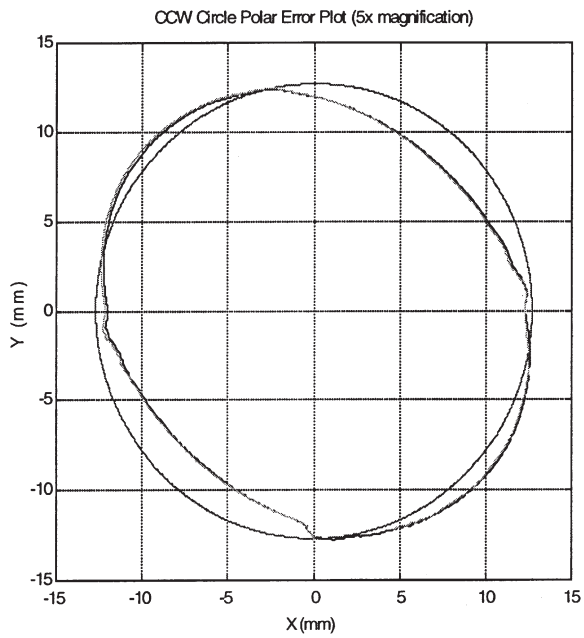

Fig. 16. Circular path comparison (1778 min/min, 4.91 m/s^2).

the measurement results did not provide the expected micrometer-level reproduction between the two measurement sets. Therefore, the dynamic repeatability of both measurement systems was evaluated. Fig. 17 shows three consecutive dynamic path measurements using the Heidenhain grid plate. It can be seen that there is approximately a 20 μm error band (parallel to the average of the measured contours) which is necessary to contain the separate measurements. Similarly, three back-to-back contours measured with the STLBB are shown in Fig. 18. In this case, a roughly 15 μm error band is recognized. Because the grid plate is a non-contact device, it cannot affect the machine tool's dynamic performance. Therefore, the contouring non-repeatability of the measured motions was due to the dynamic non-repeatability of the machine tool and not the measurement systems. The machine tool dynamic non-repeatability, therefore, served as a lower bound on the accuracy of the measurement comparison.

Static positioning repeatability tests were also completed. For these measurements, STLBB results were compared to those obtained using a capacitance probe setup. Sub-micrometer level agreement was found. The interesting conclusion from these measurements was that the machine used in this study behaved well statically, but poorly dynamically.

4. Three-dimensional contour measurements

Several paths, which combined both linear and circular interpolation, were chosen to investigate the STLBB 3-D measurement performance. Two will be shown here. The first path, displayed with an STLBB measurement in Fig. 19, is corkscrew in nature. For this corkscrew path, a counter-clockwise half-circle was commanded in the *x-y* plane, then a small step in the *-z* direction

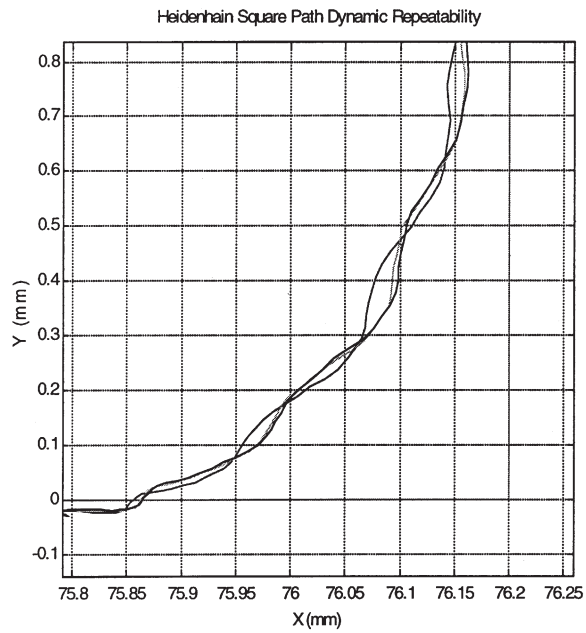

Fig. 17. Heidenhain dynamic repeatability test.

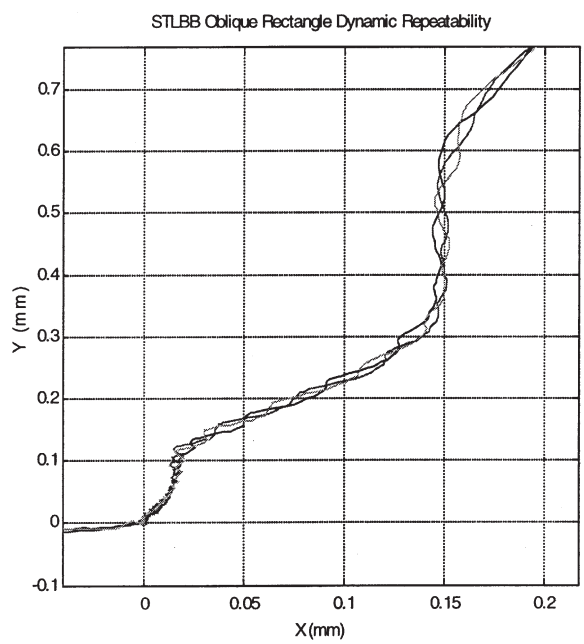

Fig. 18. STLBB dynamic repeatability test.

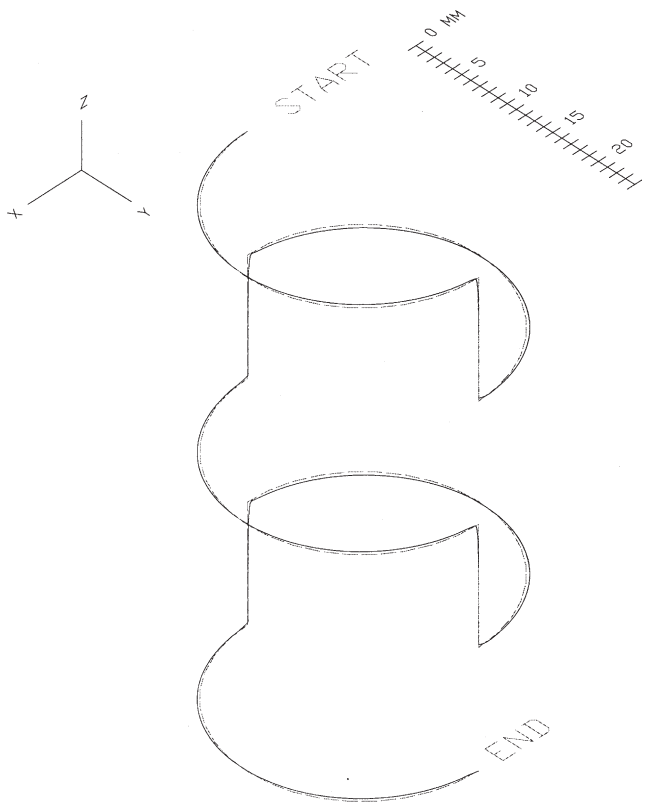

Fig. 19. STLBB corkscrew path.

was executed. Next, another half-circle was completed and followed by another step in the -z direction, and so on.

In Fig. 20, the transition from the first half-circle to the first -z motion in the corkscrew path is shown. The elliptical distortion of the half-circle in the x-y plane is evident as well as undershoot in both the x and y directions for the start of the -z motion. The integral gain in the controller then begins to correct the steady state error in the x and y directions as the z motion progresses.

The second path is a rectangle located on a plane oblique to the three axes of the machine. Fig. 21 shows the commanded contour and two different measurement results at feed rates of 889 mm/min and 1778 mm/min. Fig. 22 displays the transition from -x, +z linear interpolation to +x, +y, +z linear interpolation. The figure shows both a steady state contouring error in the x-z plane and undershoot during the cornering motion.

5. Conclusions

In this research, the application of high-speed milling to prototype production was discussed. First, the fundamental requirements for high-speed milling were outlined. These included a high speed/high power spindle, proper spindle speed selection based on system dynamics, machining

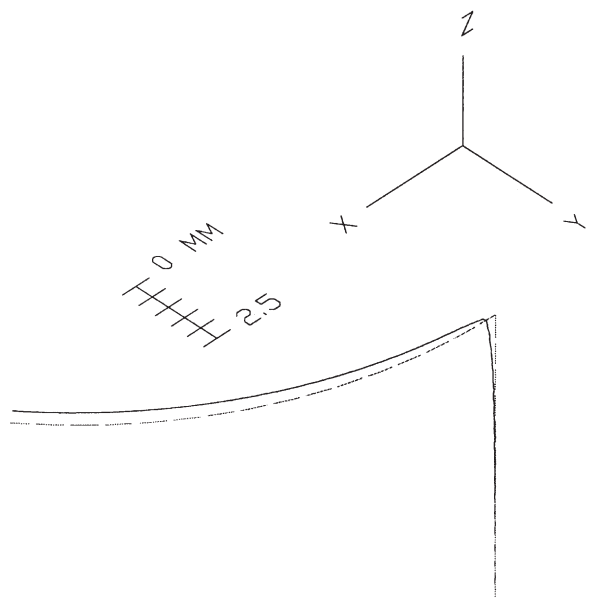

Fig. 20. STLBB corkscrew path section.

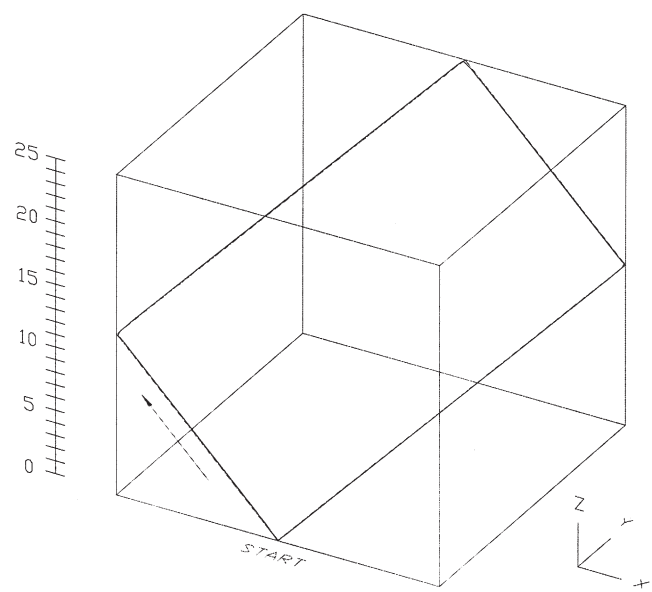

Fig. 21. STLBB oblique rectangle path.

parameter definition based on tool wear, high feed/high acceleration machine drives, and appropriate path generation. Next, the possible process time reduction made available by the use of high-speed milling was demonstrated for a generic prototype and the results tabulated. Finally, the implementation of simultaneous trilateration to measure three-dimensional CNC contours and pro-

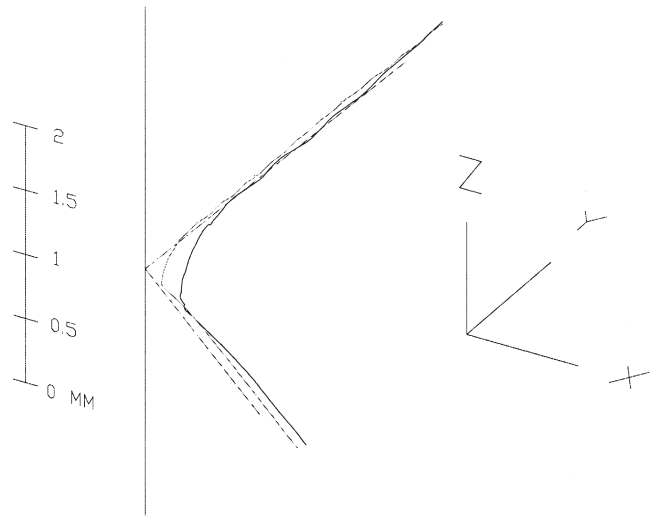

Fig. 22. STLBB oblique rectangle path section.

vide pre-process path verification using the Simultaneous Trilateration Laser Ball Bar system was shown. The verification procedure for this device was outlined and example two and three-dimensional path measurements were given. Good agreement between STLBB results and those obtained by an independent device (for 2-D contours) was recorded.

Future research may focus on such issues as: 1) a comparison of dimensional integrity between parts manufactured by standard rapid prototyping techniques and high-speed milling, 2) an evaluation of typical lead times associated with the various rapid prototyping methods and high-speed milling, 3) the role of dimensional tolerances in the final use/application of layered or machined prototypes, and 4) the final material properties of prototypes manufactured by standard rapid prototyping techniques and high-speed milling.

References

[1] D. Bourell, H. Marcus, J. Barlow, J. Beaman, Selective laser sintering of metals and ceramics, International Journal of Powder Metallurgy 28 (4) (1992) 369–381.
[2] S. Ashley, Rapid prototyping systems, Mechanical Engineering 113 (4) (1991) 34–43.
[3] P. Dickens, Research developments in rapid prototyping, Proceedings of the Institution of Mechanical Engineers Part B, Journal of Engineering Manufacture 209 (4) (1995) 261–266.
[4] X. Yan, P. Gu, A review of rapid prototyping technologies and systems, Computer-Aided Design 28 (4) (1996) 307–318.
[5] C. Chua, S. Chou, T. Wong, A study of the state-of-the-art rapid prototyping technologies, International Journal of Advanced Manufacturing Technology 14 (2) (1998) 146–152.
[6] C. Kai, 3-Dimensional rapid prototyping technologies and key development areas, Computing and Control Engineering Journal 5 (4) (1994) 200–206.
[7] D. Pham, R. Gault, A comparison of rapid prototyping technologies, International Journal of Machine Tools and Manufacture 38 (10/11) (1998) 1257–1287.
[8] K. Chin, Implementation of rapid prototyping technology — A Hong Kong manufacturing industry's perspective, International Journal of Advanced Manufacturing Technology 14 (8) (1998) 570–579.

[9] J. Tlusty, W. Zaton, F. Ismail, Stability lobes in milling, Annals of the CIRP 32 (1) (1983) 309–313.
[10] Y. Altintas, E. Budak, Analytical prediction of stability lobes in milling, Annals of the CIRP 44 (1) (1995) 357–362.
[11] S. Smith, J. Tlusty, Stabilizing chatter by automatic spindle speed regulation, Annals of the CIRP 41 (1) (1992) 433–436.
[12] W. Winfough, S. Smith, Automatic selection of the optimum metal removal conditions for high-speed milling, Transactions of the NAMRI/SME 23 (1995) 163–168.
[13] S. Smith, J. Tlusty, Current trends in high-speed machining, Transactions of the ASME Journal of Engineering for Industry 119 (1997) 664–666.
[14] S. Smith, J. Tlusty, An overview of modeling and simulation of the milling process, Transactions of the ASME Journal of Engineering for Industry 113 (1991) 169–175.
[15] Machining Data Handbook, 3rd Ed., Vol. 1 and 2, Metcut Research Associates Inc., Cincinnati, Ohio (1980).
[16] M. Davies, T. Burns, T. Schmitz, High-speed machining processes: dynamics on multiple scales. Proceedings-Dynamics and Control of Mechanical Processing (Workshop Organized by Working Group 2 Nonlinear Dynamics and Control in COST Action P4), Technical University of Budapest, Department of Applied Mechanics, Hungary, November 12–13, (1999) pp. 7–19.
[17] R.F. Recht, Catastrophic thermoplastic shear, Journal of Applied Mechanics 31 (1964) 189–193.
[18] H. Schultz, T. Moriwaki, High-speed machining, Annals of the CIRP 41 (2) (1992) 637–643.
[19] M. Weck, Y. Altintas, C. Beer, CAD assisted chatter-free NC tool path generation in milling, International Journal of Machine Tools and Manufacture 34 (6) (1994) 879–891.
[20] S. Smith, D. Dvorak, Tool path strategies for high speed milling aluminum workpieces with thin webs, Mechatronics 8 (4) (1998) 291–300.
[21] J. Bobrow, NC machine-tool path generation from CSG part representations, Computer-Aided Design 17 (2) (1985) 69–76.
[22] Y. Suh, K. Lee, NC milling tool path generation for arbitrary pockets defined by sculptured surfaces, Computer-Aided Design 22 (5) (1990) 273–284.
[23] R.-S. Lin, Y. Koren, Efficient tool-path planning for machining free-form surfaces, Transactions of the ASME Journal of Engineering for Industry 118 (1996) 20–28.
[24] M. Greul, T. Pintat, M. Greulich, Rapid prototyping of functional metallic parts, Computers in Industry 28 (1) (1995) 23–28.
[25] Y. Chen, Y. Hu, Implementation of a robot system for sculptured surface cutting. Part 1. Rough machining, International Journal of Advanced Manufacturing Technology 15 (9) (1999) 624–629.
[26] Y. Chen, Y. Hu, Implementation of a robot system for sculptured surface cutting. Part 2. Finish machining, International Journal of Advanced Manufacturing Technology 15 (9) (1999) 630–639.
[27] N. Shiomi, A. Yoshidome, F. Abe, K. Osakada, Finite element analysis of melting and solidifying processes in laser rapid prototyping of metallic powders, International Journal of Machine Tools and Manufacture 39 (2) (1998) 237–252.
[28] J. Halley, A. Helvey, S. Smith, W. Winfough, The impact of high-speed machining on the design and fabrication of aircraft components. Proceedings of the 17th Biennial Conference on Mechanical Vibration and Noise (DETC99/VIB-8057), 1999 ASME Design and Technical Conferences, Las Vegas, Nevada, September 12–15, (1999) pp. 1–5.
[29] R. Komanduri, J. McGee, R. Thompson, J. Covy, F. Truncale, V. Tipnis, R. Stach, R. King, On a methodology for establishing the machine tool system requirements for high-speed/high-throughput machining, Transactions of the ASME Journal of Engineering for Industry 107 (1985) 316–324.
[30] T. Schmitz, J. Ziegert, A new sensor for the micrometre-level measurement of three-dimensional, dynamic contours, Measurement Science and Technology 10 (2) (1999) 51–62.
[31] H. Soons, S. Yaniv, Precision in Machining: Research Challenges, NISTIR 5628. National Institute of Standards and Technology, May (1995).
[32] T. Schmitz, The implementation of simultaneous trilateration to measure dynamic three-dimensional contours using the laser ball bar. PhD dissertation, University of Florida, Gainesville, FL, May (1999).
[33] J. Ziegert, C. Mize, Laser ball bar: a new instrument for machine tool metrology, Precision Engineering 16 (4) (1994) 259–267.

[34] C. Mize, J. Ziegert, R. Pardue, N. Zucker, Spatial Measurement Accuracy Tests of the Laser Ball Bar. Final Report for CRADA No. Y-1293-02244 between Martin Marietta Energy Systems and Tetra Precision, Inc., August (1994).